2-28-2023

Toll-like Receptor 4 Signaling in Osteoblasts Is Required for Load-Induced Bone Formation in Mice

Ibtesam Rajpar
Thomas Jefferson University

Gaurav Kumar
Thomas Jefferson University

Paolo Fortina
Thomas Jefferson University

Ryan E. Tomlinson
Thomas Jefferson University

iScience

CellPress
OPEN ACCESS

Article

Toll-like receptor 4 signaling in osteoblasts is required for load-induced bone formation in mice

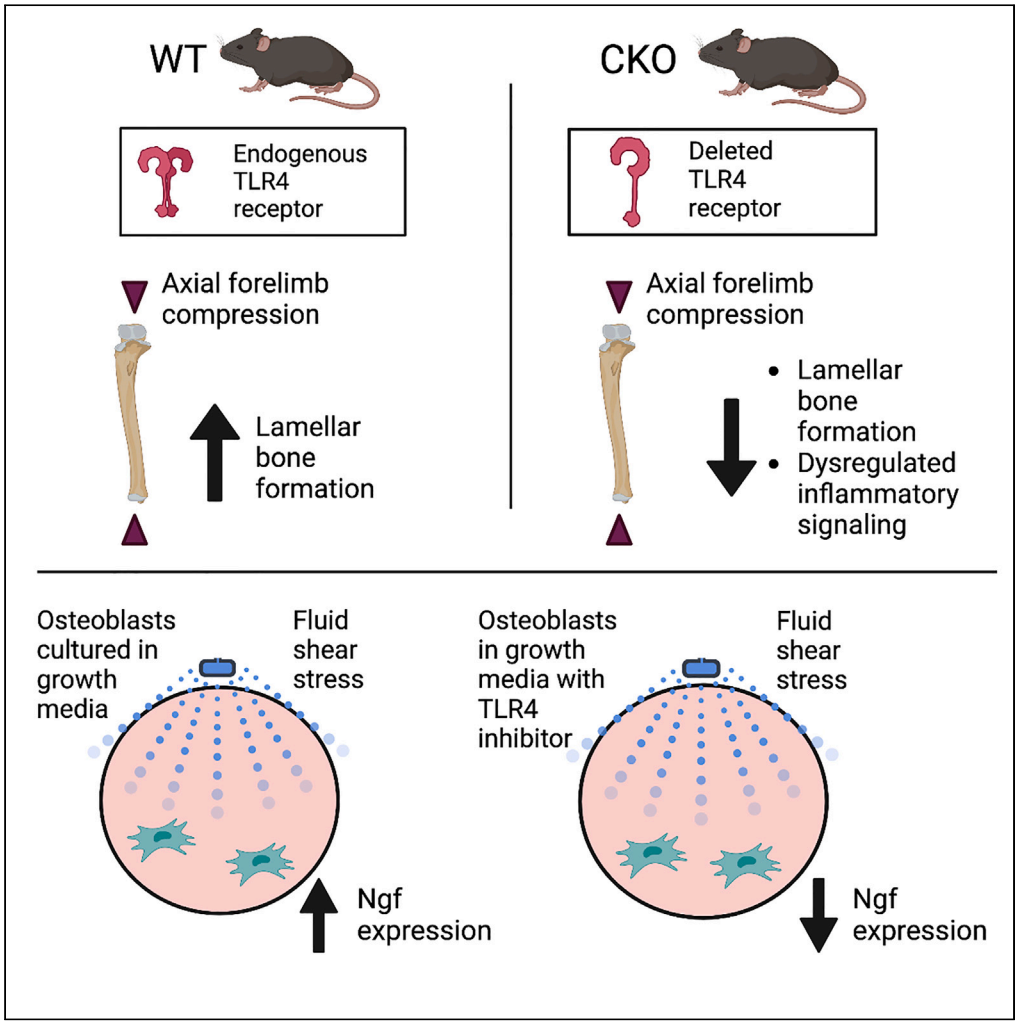

Ibtesam Rajpar, Gaurav Kumar, Paolo Fortina, Ryan E. Tomlinson

ryan.tomlinson@jefferson.edu

Highlights

Inhibition of NF-κB signaling reduces osteoblastic NGF expression following loading

Mice lacking *Tlr4* in mature osteoblasts have reduced load-induced bone formation

Upregulation of *Ngf* following fluid shear stress is abrogated by TLR4 inhibition

Load-induced inflammatory signaling is dysregulated in *Tlr4* conditional knockout mice

Rajpar et al., iScience *26*, 106304
April 21, 2023
https://doi.org/10.1016/j.isci.2023.106304

iScience

CellPress
OPEN ACCESS

Article

Toll-like receptor 4 signaling in osteoblasts is required for load-induced bone formation in mice

Ibtesam Rajpar,[1] Gaurav Kumar,[2] Paolo Fortina,[2] and Ryan E. Tomlinson[1,3,*]

SUMMARY

In mature bone, NGF is produced by osteoblasts following mechanical loading and signals through resident sensory nerves expressing its high affinity receptor, neurotrophic tyrosine kinase receptor type 1 (TrkA), to support bone formation. Here, we investigated whether osteoblastic expression of Toll-like receptor 4 (TLR4), a key receptor in the NF-κB signaling pathway, is required to initiate NGF-TrkA signaling required for load-induced bone formation. Although *Tlr4* conditional knockout mice have normal skeletal mass and strength in adulthood, the loss of TLR4 signaling significantly reduced lamellar bone formation following loading. Inhibition of TLR4 signaling reduced *Ngf* expression in primary osteoblasts and RNA sequencing of bones from *Tlr4* conditional knockout mice and wild-type littermates revealed dysregulated inflammatory signaling three days after osteogenic mechanical loading. In total, our study reveals an important role for osteoblastic TLR4 in the skeletal adaptation of bone to mechanical forces.

INTRODUCTION

The skeleton is constantly subjected to various compressive, tensile, and shear forces. The cellular constituents of bone, namely the osteoblasts and osteocytes, respond to these loads by depositing new bone at regions of high strain and removing bone at regions of low strain, in a process known as strain-adaptive bone remodeling.[1,2] Thus, remodeling of bone tissue is achieved by the conversion of mechanical cues to biochemical signals by bone cells.[3] One mechanism by which these signals are perceived is through the dense network of peripheral nerves present on the mammalian bone surface.[4] The vast majority of these nerves express the neurotrophic tyrosine kinase receptor type I (TrkA),[5,6] which is the high affinity receptor for the classic neurotrophin nerve growth factor (NGF).[7] During development, NGF is produced by osteochondral progenitors as part of a developmental program to specify the amount and type of innervation required in bone.[8] In adulthood, NGF is also produced by mature osteoblasts in response to loading, and NGF-TrkA signaling is required to achieve maximal load-induced bone formation.[9,10] As a result, inhibition of TrkA signaling in adult mice significantly reduces bone formation following axial forelimb compression.[10] Furthermore, exogenous NGF injection in wild-type (WT) mice increases load-induced bone formation rate and Wnt signaling in osteocytes.[10] However, more investigation is needed to understand the control of NGF expression by osteoblasts involved in a well-orchestrated anabolic response to loading.

Previous studies have observed that nuclear factor κB (NF-κB) signaling is rapidly activated in osteoblastic cells by mechanical forces.[11–13] For example, application of fluid shear stress to osteoblasts results in the rapid increase of intracellular calcium, which is required for the release and nuclear translocation of NF-κB factors to activate the production of prostaglandins.[13] Generally, the NF-κB factors have been associated with homeostatic functions in bone, primarily catabolic bone resorption,[14] although a recent study showed that the constitutive activation of NF-κB signaling in osterix-expressing cells increased overall bone mass through enhanced basal and load-induced bone formation.[15] Importantly, NF-κB activation is specifically required for B cell-derived and NP-cell-derived NGF expression[16,17] and activation of NF-κB factors promotes the NGF-mediated survival of sympathetic neurons.[18] In total, these studies strongly suggest a role for NF-κB signaling in the transcriptional activation of *Ngf* in mature osteoblasts following osteoanabolic mechanical loading.

[1]Department of Orthopaedic Surgery, Thomas Jefferson University, Philadelphia, PA, USA

[2]Department of Cancer Biology, Thomas Jefferson University, Philadelphia, PA, USA

[3]Lead contact

*Correspondence: ryan.tomlinson@jefferson.edu

https://doi.org/10.1016/j.isci.2023.106304

Among potential cell surface receptors associated with NF-κB signaling, the Toll-like receptors (TLRs) have been classically associated with the maintenance of innate immunity but are also expressed in a variety of cells in the musculoskeletal lineage including chondrocytes, synoviocytes, and osteoblasts.[19] Here, we focus on TLR4—a type I transmembrane receptor with an extracellular domain comprising 19–25 copies of the leucine-rich repeat motif that recognizes highly conserved molecular patterns of evolutionary origin, such as the classic lipopolysaccharide and high-mobility group box protein 1.[20] In bone, TLR4 activation has been linked to the increased expression of RANKL and M-CSF.[21] These signaling factors are activated during osteoclastogenesis and promote bone resorption, but also increase secretion of the osteoanabolic Wnts (Wnt3a and Wnt5a) to promote osteogenic differentiation, proliferation, and angiogenesis.[19,22] Analogous to the NF-κB signaling proteins, the TLR4 receptor is activated in response to mechanical stimulation.[23] In a previous study with healthy human disc cells, both TLR2 and TLR4 agonists were found to increase NGF gene expression following treatment.[17,24] Furthermore, inhibition of NF-κB signaling with a small molecule inhibitor in disc cells silenced TLR2-driven NGF expression at both the gene and protein levels.[17] Therefore, we hypothesized that activation of TLR4 in osteoblasts drives NF-κB signaling to promote the NGF expression required for normal bone formation in response to mechanical loading.

To investigate this hypothesis, we developed a conditional knockout mouse line in which *Tlr4* was specifically removed from the mature osteoblast lineage using osteocalcin Cre-mediated recombination. We analyzed the skeletal phenotype of these mice as well as load-induced bone formation and the transcriptional response following axial forelimb compression. We further investigated our hypothesis using an *in vitro* model of fluid shear stress in which osteoblasts were treated with various NF-κB inhibitors and a TLR4-specific inhibitor to determine the requirement of NF-κB signaling factors and the TLR4 receptor in the response to loading. Our findings reveal novel mechanistic insights to the NGF-TrkA signaling pathway in bone, and a new role of the TLRs in osteoanabolic loading.

RESULTS

Loading increases TLR4+ periosteal cells as well as NGF expression that is blocked by NF-κB inhibition

To determine the requirement of NF-κB signaling for NGF expression in bone following axial forelimb compression, we administered the NF-κB inhibitor BAY 11-7082 (20 mg/kg, Cayman Chemicals) or vehicle (DMSO) to adult NGF-EGFP mice 1 h before a single bout of axial forelimb compression. By confocal microscopy, we observed robust NGF expression at the periosteal surface 3 h after loading that was essentially silenced by the inhibitor (Figures 1A and 1B). Quantification of the area of GFP expression in the periosteal region revealed a significant (−73%) decrease in the mice treated with BAY 11-7082. Next, mRNA was harvested 24 h after loading for analysis by qRT-PCR. Here, we found that treatment with BAY 11-7082 was associated with significant decreases in *Ngf* (−52%), *Wnt1* (−37%), and *Wnt7b* (−46%), such that they were not different than control (non-loaded) limbs (Figures 1D–1F). In addition, *Nfkb1* was significantly decreased (−44%) in mice treated with BAY 11-7082 (Figure 1G). Since NF-κB signaling can be activated through TLRs, including TLR4, we examined the expression of TLR4 in loaded and non-loaded forelimbs using immunohistochemistry 7 days after axial forelimb compression. Here, we observed that the number of TLR4+ periosteal cells was significantly increased in loaded limbs (Figures 1H–1J). In total, these data suggested that NF-κB signaling following loading induced NGF expression and was potentiated through the activity of TLR4. To test this hypothesis, we generated TLR4 conditional knockout (CKO) mice in which exon 3 of *Tlr4* was excised by Cre-mediated recombination under the control of the full-length osteocalcin promoter.

Adult bone mass and strength is not affected by loss of TLR4 in the mature osteoblast lineage

TLR4 CKO mice appeared healthy and fertile and were obtained at the expected Mendelian frequency. The genotype of the mice was confirmed by amplification of genomic DNA. Furthermore, ulna bones from CKO mice had significantly less *Tlr4* mRNA as compared to WT mice, with no significant differences in *Tlr4* expression in kidney, muscle or skin (Figures S1A–S1D). Alizarin red and Alcian blue skeletal preparations of neonates at postnatal day 0 revealed no significant differences in the size or shape of skeletal elements (Figure S2). Paraffin sections of adolescent (8–9 weeks) femurs were analyzed to assess changes in cellular composition of CKO mice. While no changes were noted in numbers of osteoblasts or osteocytes, TRAP staining revealed a significantly reduced number of osteoclasts (−25%) in CKO metaphyseal bone as compared to WT littermates (Figure S3). Next, we analyzed adult bone mass and geometry using femurs harvested from 16- to 20-week-old mice. MicroCT revealed no significant differences in trabecular or

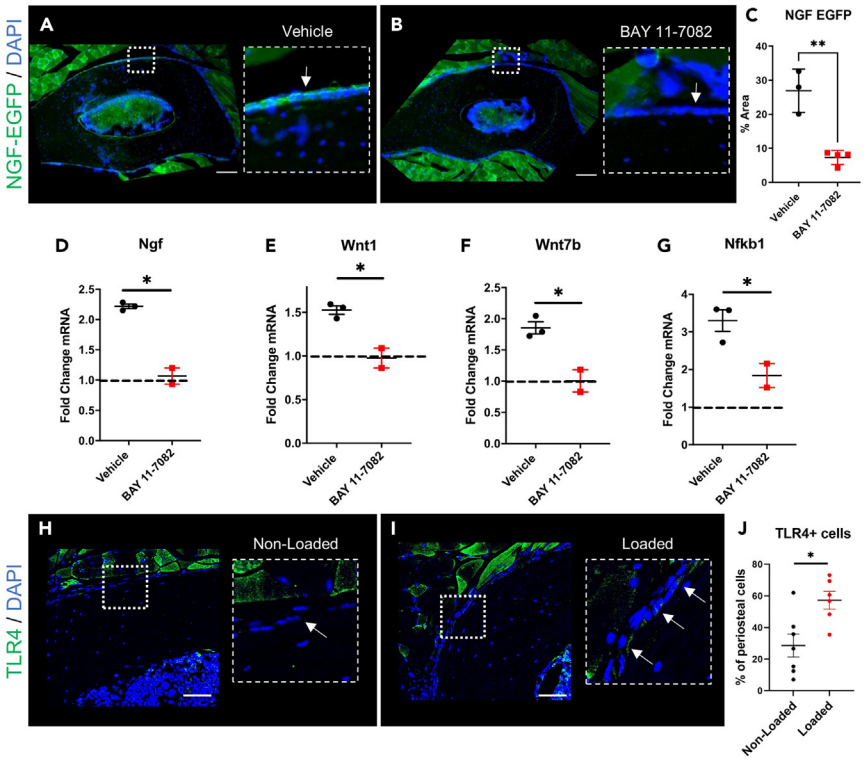

Figure 1. Loading increases NGF expression that is blocked by NF-κB inhibition as well as TLR4+ periosteal cells

(A–G) (A) Expression of NGF in the periosteum (arrow) of loaded ulna from NGF-EGFP mice was reduced by administration of (B) BAY 11-7082, an NF-κB signaling inhibitor, with (C) quantification of the % area of GFP expression 3 h after loading. Scale bars are 100 microns. Similarly, (D) *Ngf*, (E) *Wnt1*, (F) *Wnt7b*, and (G) *Nfkb1* expression were significantly decreased 24 h after loading.

(H–J) (H) Expression of TLR4 in the periosteum (arrow) of non-loaded and (I) loaded ulna 7 days after loading revealed a significant increase the number of TLR4+ cells, with (J) quantification of the % of TLR4+ periosteal cells 7 days after loading. Scale bars are 50 microns. *adjusted $p < 0.05$ vs. control by t-test. Data are represented as mean ± SEM.

cortical bone parameters in either male or female WT and CKO mice (Figures S4 and S5). Similarly, femoral three-point bending did not reveal any significant differences in ultimate stress, Young's modulus, or ultimate bending energy in CKO femurs compared to WT (Figure S6). In total, constitutive loss of TLR4 in the mature osteoblast lineage did not significantly affect osteoblasts, osteocytes, bone mass, or bone strength during development or in adulthood.

Osteoblastic TLR4 is required for load-induced bone formation

To directly test our hypothesis that signaling through TLR4 contributes to the osteoanabolic response following mechanical loading, male and female CKO mice were subjected to three consecutive days of axial forelimb compression. Forelimbs labeled with calcein and alizarin red were harvested 10 days after loading for analysis by dynamic histomorphometry. Here, we observed robust lamellar bone formation on the periosteal and endosteal bone surfaces of the ulnar mid-diaphysis in loaded limbs harvested from WT mice (Figures 2A and 2I), including significant increases in mineralizing surface per bone surface (MS/BS), mineral apposition rate (MAR), and bone formation rate per bone surface (BFR/BS) in loaded limbs compared to non-loaded contralateral control limbs (Table 1). However, the loss of TLR4 greatly diminished the anabolic response, with relative (loaded – non-loaded) periosteal BFR/BS significantly reduced (−50%) in male CKO mice following loading (Figure 2E). In female mice, we observed similar response to loading in WT forelimbs, but female CKO mice had even larger reductions in relative periosteal (−68%) and endosteal (−47%) BFR/BS (Figures 2M and 2P), which was mainly driven by decreases in MAR (−67%) as compared to WT littermates (Figure 2L). In non-loaded limbs, bone formation parameters were not significantly different between genotypes (Table 1). In total, these data demonstrate that osteoblastic TLR4 expression is required for normal load-induced bone formation in both male and female mice.

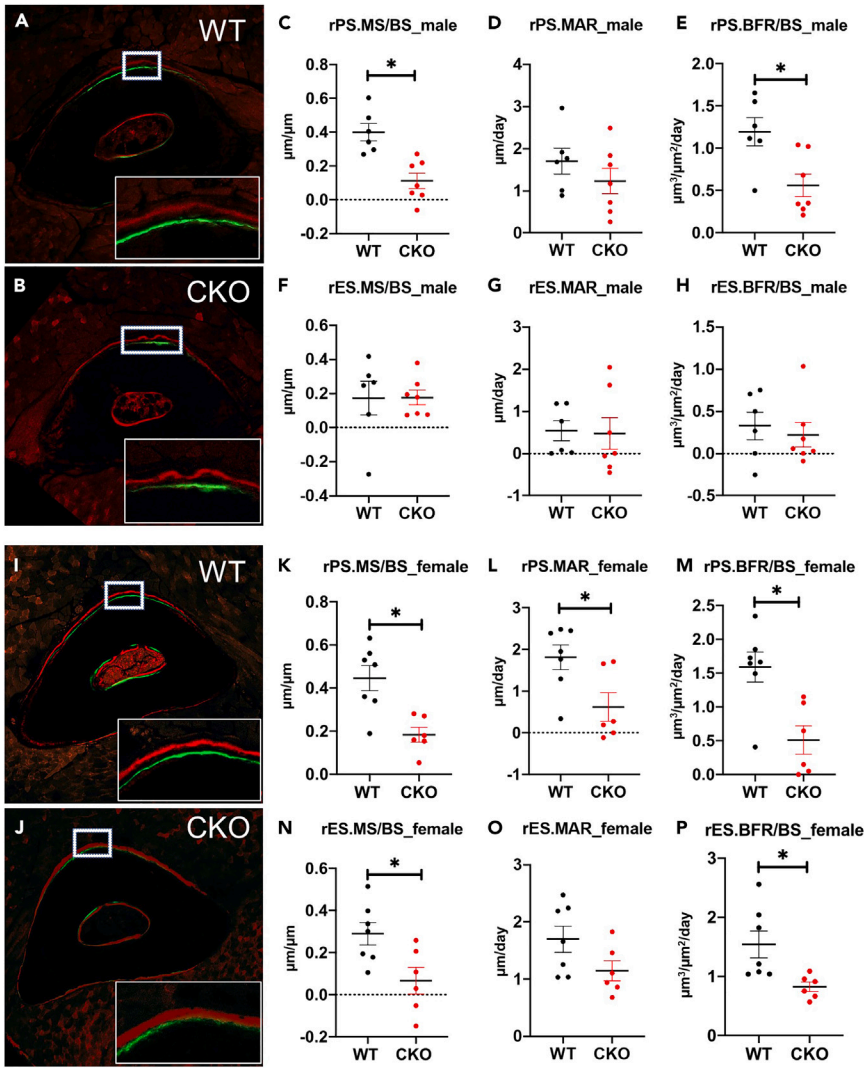

Figure 2. Tlr4 is required for lamellar bone formation following compressive forelimb loading

(A–P) Impaired bone formation following loading in *Tlr4* conditional knockout mice is demonstrated by representative cross-sections from the ulnar mid-diaphysis of (A) WT and (B) CKO male mice with quantification of (D–F) periosteal and (F–H) endosteal parameters. Similar results were obtained in females, as demonstrated by representative cross-sections from the ulnar mid-diaphysis of (I) WT and (J) CKO female mice with quantification of (K–M) periosteal and (N–P) endosteal parameters. *adjusted $p < 0.05$ between genotype by t-test. n = 6–7 per group. Data are represented as mean ± SEM.

Loss of TLR4 signaling in osteoblasts reduced *Ngf* expression following fluid shear stress

Next, we assessed if activation of TLR4 signaling induced *Ngf* expression in osteoblasts by utilizing an *in vitro* model of fluid shear stress. First, we utilized MC3T3-E1 cells to determine the time course of expression of *Ngf* following the application of fluid shear stress. Here, we found incremental increases in *Ngf* transcription in response to increased duration of fluid shear stress. Specifically, *Ngf* transcription was significantly increased following 30 (+1.5-fold) and 60 min (+2.0-fold) of fluid shear stress as compared to baseline (Figure 3B). Next, we assessed mRNA expression in calvarial osteoblasts harvested from CKO neonates and WT littermates to determine baseline gene expression. Here, we observed significant downregulation of *Tlr4* (−75% vs. WT) in CKO osteoblasts as compared to WT (Figure 3C), as expected. Further differentiation of CKO osteoblasts for 14 days yielded a more uniform population of CKO osteoblasts, with an additional reduction in *Tlr4* mRNA (−90% vs. WT). To assess the requirement of the NF-κB pathway in *Ngf* expression following application of fluid shear stress, culture media of primary calvarial osteoblasts were supplemented with the NF-κB inhibitors BAY 11-7082 or PDTC.[25,26] PDTC diminished the expression of *Ngf*

Table 1. Loss of TLR4 diminished load-induced bone formation in both female and male mice by dynamic histomorphometry

	PS.MS/BS (μm/μm)	Es.MS/BS (μm/μm)	Ps.MAR (μm/day)	Es.MAR (μm/day)	Ps.BFR/BS ($\mu m^3/\mu m^2$/day)	Es.BFR/BS ($\mu m^3/\mu m^2$/day)
FEMALE						
WT						
Loaded	0.69 ± 0.03	0.75 ± 0.03	2.78 ± 0.22*,#	2.42 ± 0.18*,#	1.93 ± 0.19*,#	1.85 ± 0.21*,#
Non-Loaded	0.24 ± 0.04	0.46 ± 0.03	0.97 ± 0.28	0.72 ± 0.15#	0.34 ± 0.10	0.31 ± 0.05#
CKO						
Loaded	0.46 ± 0.06	0.56 ± 0.06	1.58 ± 0.37	2.16 ± 0.2*	0.86 ± 0.22	1.38 ± 0.17*
Non-Loaded	0.28 ± 0.07	0.49 ± 0.07	0.96 ± 0.25	1.02 ± 0.24	0.35 ± 0.07	0.56 ± 0.14
MALE						
WT						
Loaded	0.57 ± 0.01	0.44 ± 0.09	2.46 ± 0.34*	1.03 ± 0.21#	1.38 ± 0.18*,#	0.57 ± 0.13
Non-Loaded	0.17 ± 0.04	0.26 ± 0.07	0.75 ± 0.34	0.49 ± 0.15	0.18 ± 0.04	0.24 ± 0.07
CKO						
Loaded	0.42 ± 0.03	0.31 ± 0.05	1.99 ± 0.34*	0.79 ± 0.36	0.81 ± 0.15	0.32 ± 0.14
Non-Loaded	0.31 ± 0.03	0.12 ± 0.02	0.76 ± 0.15	0.31 ± 0.07	0.25 ± 0.04	0.09 ± 0.01

Values are presented as mean ± standard deviation. *p < 0.01 vs. non-loaded, #p < 0.01 vs. CKO by two-way ANOVA.

(−40%) in calvarial osteoblasts at 1 h following 60 min of loading (Figure 3D) and abolished the increase in *RelB* observed following loading (Figure 3E), but *Nfkb1* expression was not significantly affected (Figure 3F). Finally, to delineate the specific role of the NF-κB pathway receptor TLR4, cells were treated with TAK-242, a small-molecule TLR4 inhibitor.[27] In this experiment, *Ngf* expression was significantly increased (+92%) in MC3T3-E1 cells following fluid shear stress and significantly reduced by the inhibitor in a dose-dependent manner. Specifically, *Ngf* transcription was decreased −33% with 5 μM ($p = 0.0484$) and −67% with 10 μM ($p = 0.0045$) of TAK-242 (Figure 3G). We also observed that load-induced upregulation of *Ngf* transcription was reduced in CKO primary calvarial osteoblasts treated with 10 μM TAK prior to loading (Figure 3H). Although *Tlr4* expression in MC3T3-E1 cells was increased in response to fluid shear stress ($p = 0.055$), the expression level was not significantly affected by inhibition of TLR4 signaling (Figure 3I). In total, these data demonstrate that inhibition of TLR4 activity impairs *Ngf* expression in osteoblasts following fluid shear stress.

Loss of *Tlr4* in bone dysregulates inflammatory signaling following loading

To further characterize the role of osteoblastic TLR4 in osteogenic mechanical loading, mRNA was isolated from the middle third of loaded and non-loaded ulnae harvested from both CKO and WT littermates 3 h after a single bout of axial forelimb compression. RNA sequencing revealed 200 transcripts that were differently expressed (fold change >2 and an adjusted p value of ≤0.05) between loaded and non-loaded bones of WT and CKO mice (Table S1). Principal component analysis (PCA) of all groups revealed clustering within groups but relatively little separation between groups—loading induced a shift in the distribution in WT and CKO bones, mainly along PC1 (Figure S7). Nonetheless, PCA of loaded and non-loaded bone within each genotype illustrates distinct clustering, with PC1 accounting for 30.1% and PC2 accounting for 21.5% of the total variance (Figure 4A). However, individual genes accounted for relatively small percentages of the total variance—specifically, the genes *Mipepos*, *Gm37780*, and *Rnu3a.1*—accounted for ~2.5% of PC1 (Figure 4A).

Nonetheless, several differentially expressed transcripts were significantly upregulated in loaded bone when compared to non-loaded, including known mechanoresponsive genes such as *FosB* (+8.0X), *Wnt1* (+10.3X), and *Ngf* (+5.7X) (Figure 4C). In *Tlr4* CKO mice, osteoanabolic genes such as *Dmp1* (+3.1X), *Bmp4* (+2.5X), and *Bmp7* (+2.1X) were also significantly upregulated in loaded limbs. Gene set enrichment analysis was performed to identify the relevant biological pathways responsive to loading (Table S2). Here, we observed significant upregulation of WNT ($p = 0.008$) and TGFβ ($p = 0.000$) signaling following loading in both genotypes of mice (Figure 4D). In contrast, several inflammatory pathways, including IL2 ($p = 0.026$),

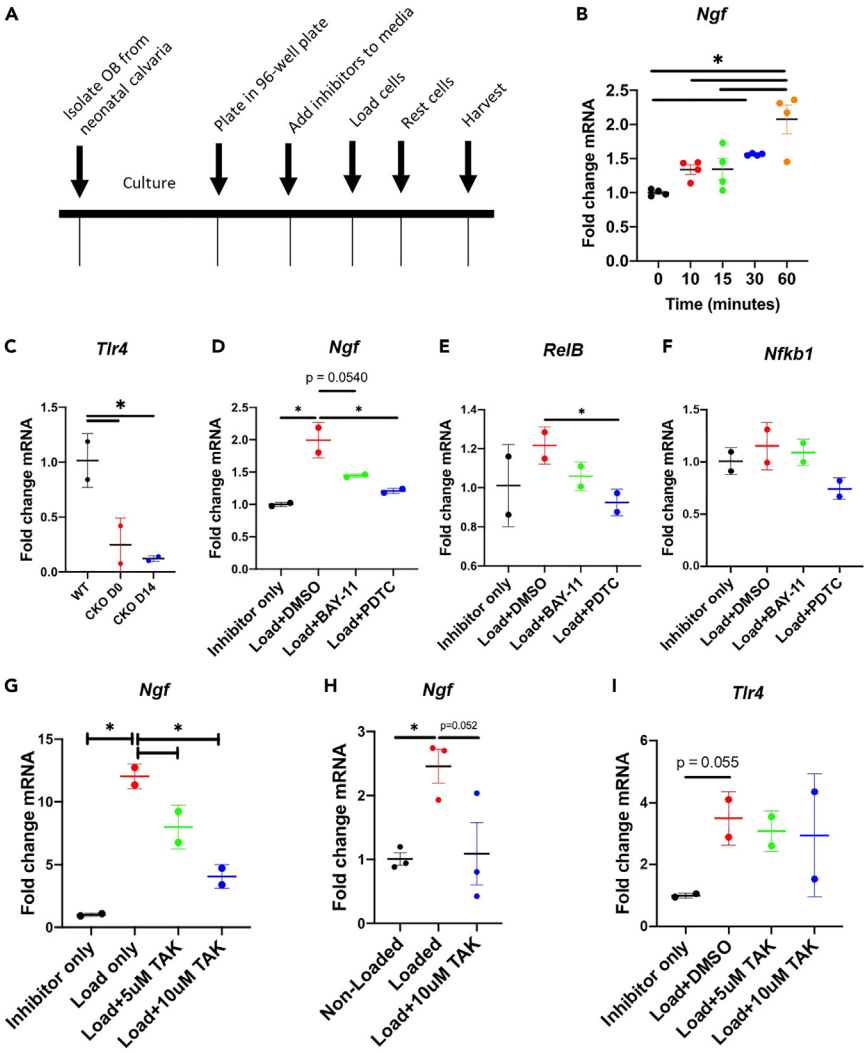

Figure 3. TLR4 signaling is required for upregulation of *Ngf* following fluid shear stress in osteoblasts

(A) Timeline illustrates the study design.

(B) Expression of *Ngf* 0–60 min after loading in MC3T3 cells.

(C) Gene expression of *Tlr4* in D0 and D14 differentiated CKO osteoblasts as compared to wild type (WT) at baseline (not loaded).

(D and E) Load-induced upregulation of *Ngf* and *RelB* was significantly reduced by pretreatment with BAY11-7082 and/or PDTC prior to loading.

(F) Expression of *Nfkb1* was not affected by loading or inhibition.

(G) Load-induced upregulation of *Ngf* in MC3T3 cells was significantly reduced by TAK-242 in a dose-dependent manner.

(H) Similarly, load-induced upregulation of *Ngf* in primary osteoblasts from CKO mice was significantly reduced by TAK-242.

(I) *Tlr4* expression in MC3T3 cells was upregulated by loading, but not affected by inhibition of signaling. *adjusted $p < 0.05$ by one-way ANOVA. Data are represented as mean ± SD.

IL6 (p = 0.000), IFN gamma (p = 0.000), and IFN alpha (p = 0.000), were upregulated in WT mice but down-regulated in CKO mice following loading (Figures 6A and 6B). Surprisingly, the loss of *Tlr4* in CKO mice appears to result in the activation of signaling pathways not directly related to bone accrual following loading, such as myogenesis and adipogenesis (Figure 6A).

PCA also revealed the distinct clustering of transcripts isolated from CKO and WT non-loaded bones, with two principal components accounting for 39.5% of the total variance (Figure 5A). Here, the genes *Npy1r*

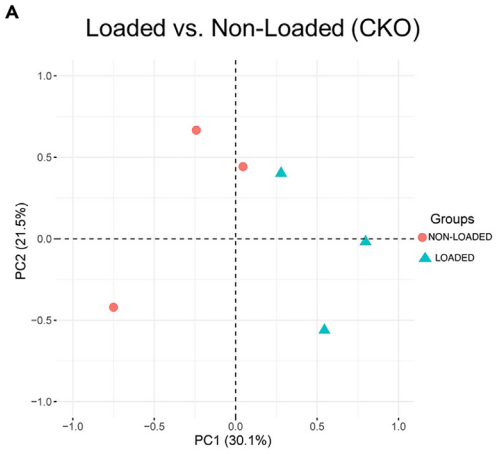

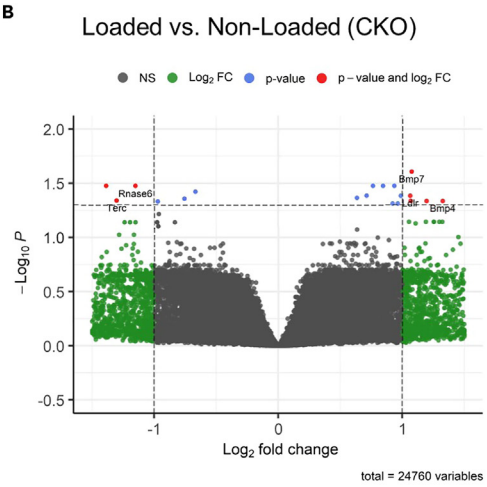

C

EFFECT OF LOAD

GENE	Fold change	p-value
Fosb	8.049170169	0.00
Bmp7	2.10343768	0.02
Bmp4	2.504940248	0.05
Wnt1	10.27559189	0.00
Ngf	5.724927134	0.00
Dmp1	3.145270231	0.00
Ldlr	2.088590904	0.04
Egr3	2.632266637	0.00
Fgf1	2.094667583	0.05
Egr1	3.631739274	0.00
Sema3d	2.288529446	0.05

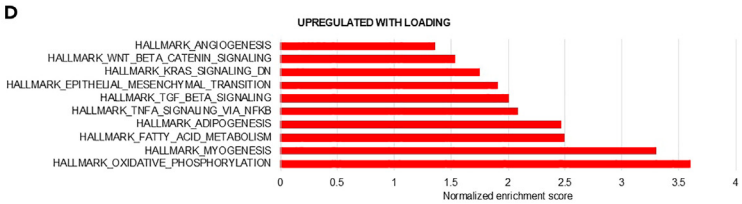

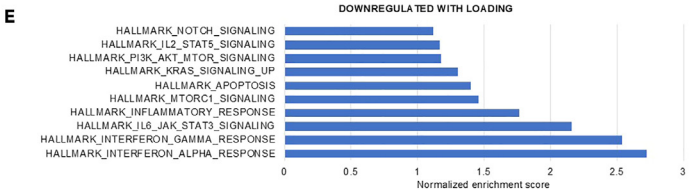

Figure 4. Loading induced significant changes in the bone transcriptome of CKO mice

RNA sequencing was performed on loaded and non-loaded forelimbs from CKO adult mice harvested 3 h following loading.

(A) Principal component analysis of loaded vs. non-loaded bones.

(B) Volcano plot of differentially expressed transcripts following loading.

(C–E) (C) Subset of differentially expressed genes relevant to anabolic response to loading. Relevant signaling pathways that were significantly (D) upregulated or (E) downregulated following loading. n = 3 per group.

and *Actr3b* accounted for ~1.6% of PC1 variance each. We observed 161 differentially expressed gene transcripts, with 34 significantly downregulated and 127 significantly upregulated in non-loaded bones from CKO as compared to WT (Figure 5B). Similar to the response to loading, we noted that several gene transcripts related to inflammatory signaling were aberrantly upregulated in the non-loaded limb of CKO mice, such as the inflammatory mediators *Il5ra* (+2.4X, p = 0.0003), *Hmgb3* (+2.1X, p = 0.0004), and *Tnf* (+2.0X, p = 0.0004) (Figure 5C). Furthermore, gene set enrichment analysis was used to identify numerous inflammatory processes, such as MTORC and TNFα signaling, that were significantly upregulated in CKO bones (Figure 5D). Indeed, these signaling pathways were upregulated in both loaded and non-loaded conditions in CKO mice (Figure 6C). Furthermore, the loss of *Tlr4* in CKO mice also resulted in a downregulation of a variety of signaling pathways in non-loaded conditions, including TGFβ signaling and angiogenesis (Figure 6D). In total, these data demonstrate that TLR4 signaling in the osteoblast is necessary for proper inflammatory signaling in both loaded and non-loaded bones.

DISCUSSION

In this study, we determined the requirement and specific role of osteoblastic TLR4 signaling following axial forelimb compression in mice. Specifically, we observed that loss of *Tlr4* in the osteoblast lineage did not significantly affect the size or shape of the skeleton and had minimal effects on cellular composition. However, CKO mice formed significantly less bone in response to axial forelimb compression as compared to

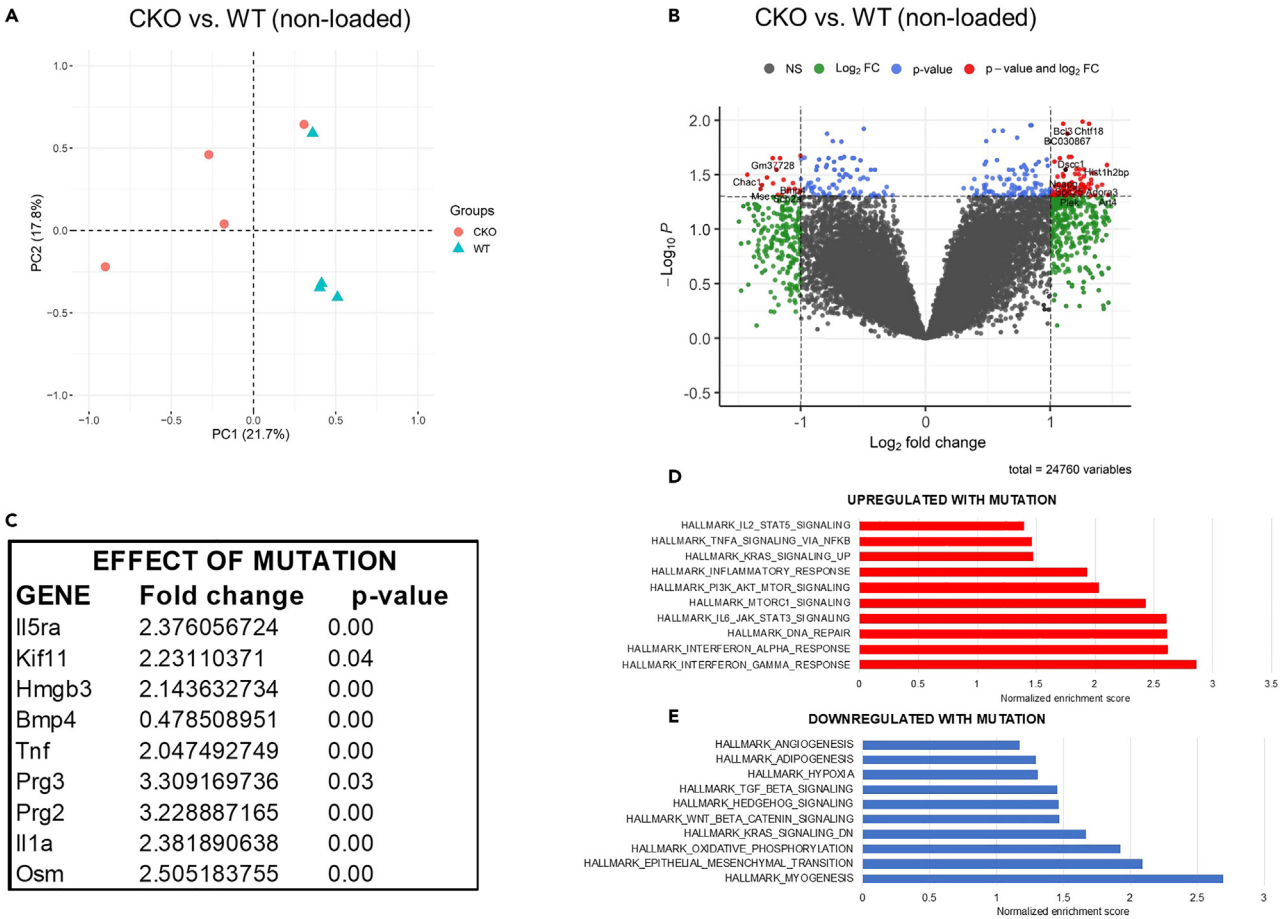

C

EFFECT OF MUTATION		
GENE	**Fold change**	**p-value**
Il5ra	2.376056724	0.00
Kif11	2.23110371	0.04
Hmgb3	2.143632734	0.00
Bmp4	0.478508951	0.00
Tnf	2.047492749	0.00
Prg3	3.309169736	0.03
Prg2	3.228887165	0.00
Il1a	2.381890638	0.00
Osm	2.505183755	0.00

Figure 5. Loss of *Tlr4* induced significant changes in the bone transcriptome

RNA sequencing was performed on wild type and CKO non-loaded forelimbs.

(A) Principal component analysis of CKO vs. WT bones.

(B) Volcano plot of differentially expressed transcripts.

(C–E) (C) Subset of differentially expressed genes relevant to the mutation. Relevant signaling pathways that were significantly (D) upregulated or (E) downregulated in CKO vs. wild type. n = 4 per group.

WT littermates, and had a dysregulated inflammatory response as demonstrated by RNA sequencing. Furthermore, we showed *in vitro* that *Ngf* expression in response to fluid shear stress was impaired in a dose-dependent manner by TLR4 inhibitors. In total, these data strongly support a model in which activation of TLR4 on mature osteoblasts supports load-induced bone formation through regulation of inflammatory signaling (Figure 7).

To pinpoint the function of TLR4 in osteoblasts during load-induced bone formation, we developed a novel conditional knockout mouse model of *Tlr4* deficiency using osteocalcin Cre-mediated deletion to target the mature osteoblast lineage. We hypothesized that the relatively late expression of osteocalcin in mature osteoblasts would circumvent potential developmental deficits due to loss of *Tlr4*. Consistent with this hypothesis, mutant CKO mice did not exhibit any differences in bone parameters as determined by microCT or material properties by standard three-point bending when compared to their WT littermates. This finding is consistent with global and myeloid-cell-specific *Tlr4* knockout models that did not report any skeletal abnormalities,[28] though loss of *Tlr4* does impact the morphology and function of the retina, cardiac function, and developmental neuroplasticity in mice.[29] However, we did observe lower numbers of osteoclasts in the trabecular bone of CKO mice (Figures S3E–S3G). This finding did not appear to affect bone mass or outcomes from mechanical loading and likely stems from the altered inflammatory signaling due to loss of osteoblastic TLR4 (Figure 5). Nonetheless, the reduced osteoclast number may be relevant

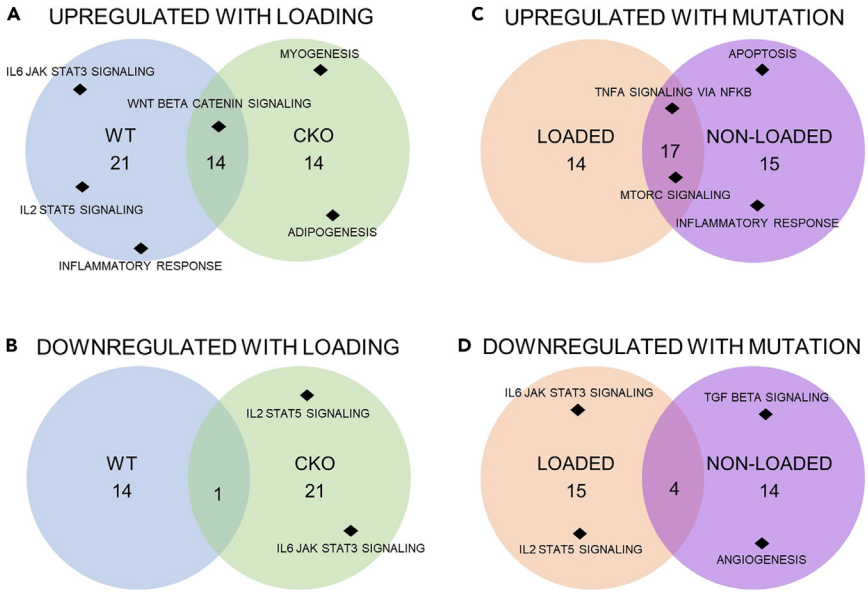

Figure 6. Common and unique hallmarks from RNA sequencing

(A–D) The number of signaling pathways (A) upregulated or (B) downregulated in WT mice, CKO mice, or both genotypes in loaded limbs as compared to non-loaded limbs. Similarly, the number of pathways (C) upregulated or (D) downregulated in loaded limbs, non-loaded limbs, or both limbs in CKO mice as compared to WT mice. A full list of the significant pathways is available in Table S2 n = 3–4 per group.

to future studies of TLR4 function in bone, particularly regarding callus remodeling following fracture. Indeed, previous studies have demonstrated that TLR4 activation is associated with bone resorption and osteoblast-mediated osteoclastogenesis during active bone remodeling and in inflammatory bone disorders.[19,30]

Furthermore, our results demonstrate that activation of TLR4 in mature osteoblasts is required for load-induced bone formation, illustrating a novel osteoanabolic function of a receptor primarily associated with inflammatory bone loss.[28] In particular, we observed increased numbers of TLR4+ cells on the ulnar periosteal surface following axial forelimb compression. More study is required to determine if these TLR4-expressing cells generated after loading are mature osteoblasts, osteoprogenitors, or non-osteoblastic cells present in periosteum.[31] To investigate sex-related differences in the response of bone to *Tlr4* knockout, both male and female mice were included in our analysis. Loss of *Tlr4* in both male and female mice resulted in similar overall reductions in the key outcome parameter following axial forelimb compression—periosteal BFR/BS. This result was mainly driven by decreased activation of osteoblasts, as demonstrated by significantly decreased MS/BS in both male and female mice; only female mice had significantly decreased MAR. Furthermore, only female mice displayed a significant reduction in endosteal BFR/BS, which was also mainly driven by decreased endosteal MS/BS. In total, it appears that loss of osteoblastic *Tlr4* affected load-induced bone formation in female mice more strongly than male mice (Figure S8), but more study is required to determine the source of this difference. Furthermore, there were no significant differences in bone formation parameters between genotypes in non-loaded limbs, underscoring that the role of TLR4 appears limited to the response to loading.

We specifically hypothesized that TLR4 signaling may be required for *Ngf* expression through NF-κB signaling in osteoblasts following mechanical loading. First, we showed that administration of NF-κB inhibitor to NGF-EGFP reporter mice silences NGF expression following axial forelimb compression. Next, we utilized a series of *in vitro* studies to show that *Ngf* expression following the application of fluid shear is significantly reduced by both BAY11-7082 and PDTC, inhibitors of the NF-κB signaling pathway, as well as TAK-242, a TLR4-specific inhibitor, in a dose-dependent manner. As a result, we were surprised to find that both WT and CKO mice displayed a significant upregulation of *Ngf* following axial forelimb compression by RNA sequencing (Table S1). Furthermore, both WT and CKO bones retained significant increases in *Wnt1* transcription in response to mechanical loading, which we have shown previously to

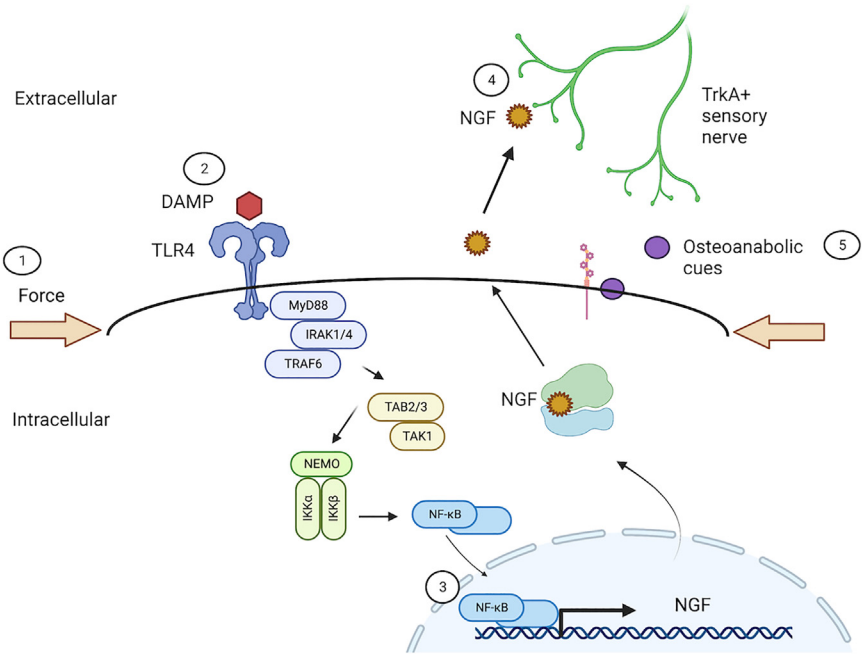

Figure 7. Schematic of TLR4 signaling in load-induced bone formation

1) Mechanical loading of osteoblasts promotes the activation of TLR4 receptors by endogenous DAMPS and/or TLR4 agonists, 2) TLR4 activation stimulates formation of the NEMO complex, resulting in the release and nuclear translocation of NF-κB factors, 3) NF-κB factors bind and activate transcription of *Ngf*, 4) NGF is released from osteoblasts and binds its high affinity receptor TrkA on skeletal sensory nerves, and 5) NGF-TrkA signaling promotes the release of osteoanabolic cues that support new bone formation.

be upregulated in response to exogenous NGF.[10] Thus, more study is required to determine if the source of NGF is the small fraction of osteoblasts that retain *Tlr4*, cells outside of the mature osteoblast lineage (e.g. inflammatory cells or osteoprogenitors), or the expression of alternative receptors to compensate for the constitutive loss of TLR4 in mature osteoblasts.

Several studies have shown that mechanical loading induces inflammatory genes that are required for a normal osteogenic response. For example, compressive loading of murine neonatal osteoblasts increases IL6 production required for bone remodeling in osteoarthritis.[32] Moreover, axial forelimb compression in rats induces vasodilation, mast cell infiltration, and the production of nitric oxide synthase.[33] In this study, CKO mice did not activate several of the inflammatory signaling pathways observed to be upregulated in WT mice following loading, including IL2, IL6, and IFNα signaling. Thus, we showed that loss of osteoblastic *Tlr4* results in a dysregulated inflammatory response, suggesting that TLRs act as regulators of the inflammation that potentiates load-induced bone mass accrual.[33] Indeed, previous studies have illustrated that activation of NGF-TrkA signaling in monocytes decreases TLR-mediated translocation of NF-κB factors and glycogen synthase kinase 3 activity, resulting in a decreased production of inflammatory cytokines.[34,35] In this study, we have not specifically investigated the downstream intracellular signaling following TLR4 activation, which may be altered following osteogenic mechanical loading or fluid shear stress. Therefore, additional studies are required to determine the specific action of TLR4 signaling regarding the proper resolution of inflammation in loaded bone.

In total, the results from this study illustrate the novel role of TLR4 signaling in mature osteoblasts to support load-induced bone formation. Furthermore, we showed that the TLR4-NGF-TrkA signaling axis in mature osteoblasts is dispensable for skeletal development but activated in response to mechanical loads to support bone formation and mediate inflammatory signaling. Future work will focus on the differentiation stage of osteoblasts that express TLR4, the specific receptor agonists required for load-induced bone formation, and the role of osteoblastic TLR4 in other skeletal contexts, such as fracture repair and osteomyelitis.

Limitations of the study

A potential limitation to the findings presented in this study is based on the selection of osteocalcin as a promoter of Cre recombination and marker of mature osteoblasts in CKO mice. A previous study has reported modest OC-Cre recombination in non-skeletal sites.[36] In this study, we observed that Tlr4 expression in skin from CKO mice appeared to trend downward as compared to WT mice, but did not reach significance (Figure S1D). Nonetheless, we do not expect non-skeletal Cre recombination would affect the outcomes reported in this study. Another limitation is the use of undifferentiated CKO osteoblasts for *in vitro* loading experiments—it is possible that some immature osteoblasts that do not express osteocalcin can contribute to Ngf expression following loading. Indeed, differentiation of CKO osteoblasts to 14 days reduced Tlr4 expression to minimal levels and was significantly different than undifferentiated CKO osteoblasts.

STAR★METHODS

Detailed methods are provided in the online version of this paper and include the following:

- KEY RESOURCES TABLE
- RESOURCE AVAILABILITY
  - Lead contact
  - Materials availability
  - Data and code availability
- EXPERIMENTAL MODEL AND SUBJECT DETAILS
  - Mouse strains
  - Cell lines and culture
- METHOD DETAILS
  - Skeletal preparations
  - *In vivo* mechanical loading
  - Histomorphometry
  - Micro computed tomography and three-point bending
  - RNA isolation and sequencing
  - *In vitro* fluid shear stress
  - Gene expression analysis
- QUANTIFICATION AND STATISTICAL ANALYSIS

SUPPLEMENTAL INFORMATION

Supplemental information can be found online at https://doi.org/10.1016/j.isci.2023.106304.

ACKNOWLEDGMENTS

Our research is supported by the National Institute of Arthritis and Musculoskeletal and Skin Diseases, the National Institute of Dental and Craniofacial Research, and the Office of the Director of the National Institutes of Health under award numbers AR074953 (RET), DE028397 (RET), and OD025128 (PF). The authors thank Dr. Michael Kawaja for supplying mice used in this study and Dr. Adam Ertel for help with data visualization. The content is solely the responsibility of the authors and does not necessarily represent the official views of the funding bodies.

AUTHOR CONTRIBUTIONS

I.R.: Conceptualization, Methodology, Investigation, Writing; G.K.: Investigation; P.M.F.: Methodology, Supervision; R.E.T.: Conceptualization, Methodology, Investigation, Supervision, Funding acquisition, Writing.

DECLARATION OF INTERESTS

The authors declare that they have no known competing financial interests or personal relationships that could have appeared to influence the work reported in this paper.

INCLUSION AND DIVERSITY

We support inclusive, diverse, and equitable conduct of research.

Received: September 2, 2022
Revised: January 6, 2023
Accepted: February 24, 2023
Published: February 28, 2023

REFERENCES

1. Christen, P., Ito, K., Ellouz, R., Boutroy, S., Sornay-Rendu, E., Chapurlat, R.D., and van Rietbergen, B. (2014). Bone remodelling in humans is load-driven but not lazy. Nat. Commun. *5*, 4855. https://doi.org/10.1038/ncomms5855.

2. Robling, A.G., and Turner, C.H. (2009). Mechanical signaling for bone modeling and remodeling. Crit. Rev. Eukaryot. Gene Expr. *19*, 319–338. https://doi.org/10.1615/critreveukargeneexpr.v19.i4.50.

3. Yavropoulou, M.P., and Yovos, J.G. (2016). The molecular basis of bone mechanotransduction. J. Musculoskelet. Neuronal Interact. *16*, 221–236.

4. Rajpar, I., and Tomlinson, R.E. (2022). Function of peripheral nerves in the development and healing of tendon and bone. Semin. Cell Dev. Biol. *123*, 48–56. https://doi.org/10.1016/j.semcdb.2021.05.001.

5. Chartier, S.R., Mitchell, S.A.T., Majuta, L.A., and Mantyh, P.W. (2018). The changing sensory and sympathetic innervation of the Young, adult and aging mouse femur. Neuroscience *387*, 178–190. https://doi.org/10.1016/j.neuroscience.2018.01.047.

6. Mach, D.B., Rogers, S.D., Sabino, M.C., Luger, N.M., Schwei, M.J., Pomonis, J.D., Keyser, C.P., Clohisy, D.R., Adams, D.J., O'Leary, P., and Mantyh, P.W. (2002). Origins of skeletal pain: sensory and sympathetic innervation of the mouse femur. Neuroscience *113*, 155–166. https://doi.org/10.1016/s0306-4522(02)00165-3.

7. Castañeda-Corral, G., Jimenez-Andrade, J.M., Bloom, A.P., Taylor, R.N., Mantyh, W.G., Kaczmarska, M.J., Ghilardi, J.R., and Mantyh, P.W. (2011). The majority of myelinated and unmyelinated sensory nerve fibers that innervate bone express the tropomyosin receptor kinase A. Neuroscience *178*, 196–207. https://doi.org/10.1016/j.neuroscience.2011.01.039.

8. Tomlinson, R.E., Li, Z., Zhang, Q., Goh, B.C., Li, Z., Thorek, D.L.J., Rajbhandari, L., Brushart, T.M., Minichiello, L., Zhou, F., et al. (2016). NGF-TrkA signaling by sensory nerves coordinates the vascularization and ossification of developing endochondral bone. Cell Rep. *16*, 2723–2735. https://doi.org/10.1016/j.celrep.2016.08.002.

9. Bleedorn, J.A., Hornberger, T.A., Goodman, C.A., Hao, Z., Sample, S.J., Amene, E., Markel, M.D., Behan, M., and Muir, P. (2018). Temporal mechanically-induced signaling events in bone and dorsal root ganglion neurons after in vivo bone loading. PLoS One *13*, e0192760. https://doi.org/10.1371/journal.pone.0192760.

10. Tomlinson, R.E., Li, Z., Li, Z., Minichiello, L., Riddle, R.C., Venkatesan, A., and Clemens, T.L. (2017). NGF-TrkA signaling in sensory nerves is required for skeletal adaptation to mechanical loads in mice. Proc. Natl. Acad. Sci. USA *114*, E3632–E3641. https://doi.org/10.1073/pnas.1701054114.

11. Granet, C., Boutahar, N., Vico, L., Alexandre, C., and Lafage-Proust, M.H. (2001). MAPK and SRC-kinases control EGR-1 and NF-kappa B inductions by changes in mechanical environment in osteoblasts. Biochem. Biophys. Res. Commun. *284*, 622–631. https://doi.org/10.1006/bbrc.2001.5023.

12. Agarwal, S., Long, P., Seyedain, A., Piesco, N., Shree, A., and Gassner, R. (2003). A central role for the nuclear factor-kappaB pathway in anti-inflammatory and proinflammatory actions of mechanical strain. FASEB J *17*, 899–901. https://doi.org/10.1096/fj.02-0901fje.

13. Chen, N.X., Geist, D.J., Genetos, D.C., Pavalko, F.M., and Duncan, R.L. (2003). Fluid shear-induced NFkappaB translocation in osteoblasts is mediated by intracellular calcium release. Bone *33*, 399–410. https://doi.org/10.1016/s8756-3282(03)00159-5.

14. Vaira, S., Johnson, T., Hirbe, A.C., Alhawagri, M., Anwisye, I., Sammut, B., O'Neal, J., Zou, W., Weilbaecher, K.N., Faccio, R., and Novack, D.V. (2008). RelB is the NF-kappaB subunit downstream of NIK responsible for osteoclast differentiation. Proc. Natl. Acad. Sci. USA *105*, 3897–3902. https://doi.org/10.1073/pnas.0708576105.

15. Davis, J.L., Cox, L., Shao, C., Lyu, C., Liu, S., Aurora, R., and Veis, D.J. (2019). Conditional activation of NF-kappaB inducing kinase (NIK) in the osteolineage enhances both basal and loading-induced bone formation. J. Bone Miner. Res. *34*, 2087–2100. https://doi.org/10.1002/jbmr.3819.

16. Heese, K., Inoue, N., and Sawada, T. (2006). NF-kappaB regulates B-cell-derived nerve growth factor expression. Cell. Mol. Immunol. *3*, 63–66.

17. Krock, E., Currie, J.B., Weber, M.H., Ouellet, J.A., Stone, L.S., Rosenzweig, D.H., and Haglund, L. (2016). Nerve growth factor is regulated by toll-like receptor 2 in human intervertebral discs. J. Biol. Chem. *291*, 3541–3551. https://doi.org/10.1074/jbc.M115.675900.

18. Maggirwar, S.B., Sarmiere, P.D., Dewhurst, S., and Freeman, R.S. (1998). Nerve growth factor-dependent activation of NF-kappaB contributes to survival of sympathetic neurons. J. Neurosci. *18*, 10356–10365.

19. Alonso-Pérez, A., Franco-Trepat, E., Guillán-Fresco, M., Jorge-Mora, A., López, V., Pino, J., Gualillo, O., and Gómez, R. (2018). Role of toll-like receptor 4 on osteoblast metabolism and function. Front. Physiol. *9*, 504. https://doi.org/10.3389/fphys.2018.00504.

20. Ng, A., and Xavier, R.J. (2011). Leucine-rich repeat (LRR) proteins: integrators of pattern recognition and signaling in immunity. Autophagy *7*, 1082–1084. https://doi.org/10.4161/auto.7.9.16464.

21. AlQranei, M.S., Senbanjo, L.T., Aljohani, H., Hamza, T., and Chellaiah, M.A. (2021). Lipopolysaccharide- TLR-4 Axis regulates Osteoclastogenesis independent of RANKL/RANK signaling. BMC Immunol. *22*, 23. https://doi.org/10.1186/s12865-021-00409-9.

22. Bruserud, Ø., Reikvam, H., and Brenner, A.K. (2022). Toll-like receptor 4, osteoblasts and leukemogenesis; the lesson from acute myeloid leukemia. Molecules *27*, 735. https://doi.org/10.3390/molecules27030735.

23. Jacobsen, T.D., Hernandez, P.A., and Chahine, N.O. (2021). Inhibition of toll-like receptor 4 protects against inflammation-induced mechanobiological alterations to intervertebral disc cells. Eur. Cell. Mater. *41*, 576–591. https://doi.org/10.22203/eCM.v041a37.

24. Krock, E., Rosenzweig, D.H., Currie, J.B., Bisson, D.G., Ouellet, J.A., and Haglund, L. (2017). Toll-like receptor activation induces degeneration of human intervertebral discs. Sci. Rep. *7*, 17184. https://doi.org/10.1038/s41598-017-17472-1.

25. Kim, K.S., Oh, D.H., Choi, H.M., Bang, J.S., Ryu, C.J., Kim, J.H., Yoo, M.C., and Yang, H.I. (2009). Pyrrolidine dithiocarbamate, a NF-kappaB inhibitor, upregulates MMP-1 and MMP-13 in IL-1beta-stimulated rheumatoid arthritis fibroblast-like synoviocytes. Eur. J. Pharmacol. *613*, 167–175. https://doi.org/10.1016/j.ejphar.2009.04.026.

26. Tan, B., Yuan, Z., Zhang, Q., Xiqiang, X., and Dong, J. (2021). The NF-kappaB pathway is critically implicated in the oncogenic phenotype of human osteosarcoma cells. J. Appl. Biomed. *19*, 190–201. https://doi.org/10.32725/jab.2021.021.

27. Yang, X., Tao, X., Qi, W., Liu, Z., Wang, Y., Han, Q., and Xu, C. (2021). TLR-4 targeting contributes to the recovery of osteoimmunology in periodontitis. J. Periodontal. Res. *56*, 782–788. https://doi.org/10.1111/jre.12877.

28. Wang, D., Gilbert, J.R., Taylor, G.M., Sodhi, C.P., Hackam, D.J., Losee, J.E., Billiar, T.R., and Cooper, G.M. (2017). TLR4 inactivation in myeloid cells accelerates bone healing of a calvarial defect model in mice. Plast. Reconstr. Surg. *140*, 296e–306e. https://doi.org/10.1097/PRS.0000000000003541.

29. Noailles, A., Kutsyr, O., Maneu, V., Ortuño-Lizarán, I., Campello, L., de Juan, E., Gómez-Vicente, V., Cuenca, N., and Lax, P. (2019). The absence of toll-like receptor 4 mildly affects the structure and function in the adult mouse retina. Front. Cell. Neurosci. *13*, 59. https://doi.org/10.3389/fncel.2019.00059.

30. Souza, P.P.C., and Lerner, U.H. (2019). Finding a toll on the route: the fate of osteoclast progenitors after toll-like receptor activation. Front. Immunol. *10*, 1663. https://doi.org/10.3389/fimmu.2019.01663.

31. Cabahug-Zuckerman, P., Liu, C., Cai, C., Mahaffey, I., Norman, S.C., Cole, W., and Castillo, A.B. (2019). Site-specific load-induced expansion of Sca-1(+)Prrx1(+) and sca-1(-)Prrx1(+) cells in adult mouse long bone is attenuated with age. JBMR Plus *3*, e10199. https://doi.org/10.1002/jbm4.10199.

32. Sanchez, C., Gabay, O., Salvat, C., Henrotin, Y.E., and Berenbaum, F. (2009). Mechanical loading highly increases IL-6 production and decreases OPG expression by osteoblasts. Osteoarthritis Cartilage *17*, 473–481. https://doi.org/10.1016/j.joca.2008.09.007.

33. Tomlinson, R.E., Shoghi, K.I., and Silva, M.J. (2014). Nitric oxide-mediated vasodilation increases blood flow during the early stages of stress fracture healing. J. Appl. Physiol. *116*, 416–424. https://doi.org/10.1152/japplphysiol.00957.2013.

34. Minnone, G., De Benedetti, F., and Bracci-Laudiero, L. (2017). NGF and its receptors in the regulation of inflammatory response. Int. J. Mol. Sci. *18*, 1028. https://doi.org/10.3390/ijms18051028.

35. Prencipe, G., Minnone, G., Strippoli, R., De Pasquale, L., Petrini, S., Caiello, I., Manni, L., De Benedetti, F., and Bracci-Laudiero, L. (2014). Nerve growth factor downregulates inflammatory response in human monocytes through TrkA. J. Immunol. *192*, 3345–3354. https://doi.org/10.4049/jimmunol.1300825.

36. Dasgupta, K., Lessard, S., Hann, S., Fowler, M.E., Robling, A.G., and Warman, M.L. (2021). Sensitive detection of Cre-mediated recombination using droplet digital PCR reveals Tg(BGLAP-Cre) and Tg(DMP1-Cre) are active in multiple non-skeletal tissues. Bone *142*, 115674. https://doi.org/10.1016/j.bone.2020.115674.

37. Kawaja, M.D., Smithson, L.J., Elliott, J., Trinh, G., Crotty, A.M., Michalski, B., and Fahnestock, M. (2011). Nerve growth factor promoter activity revealed in mice expressing enhanced green fluorescent protein. J. Comp. Neurol. *519*, 2522–2545. https://doi.org/10.1002/cne.22629.

38. Bakke, A.D., and Klein-Nulendr, J. (2012). Osteoblast isolation from murine calvaria and long bones. In Methods Mol. Biol. (Humana Press), pp. 19–29. https://doi.org/10.1007/978-1-61779-415-5_2.

39. Tomlinson, R.E., and Silva, M.J. (2015). HIF-1alpha regulates bone formation after osteogenic mechanical loading. Bone *73*, 98–104. https://doi.org/10.1016/j.bone.2014.12.015.

40. Dempster, D.W., Compston, J.E., Drezner, M.K., Glorieux, F.H., Kanis, J.A., Malluche, H., Meunier, P.J., Ott, S.M., Recker, R.R., and Parfitt, A.M. (2013). Standardized nomenclature, symbols, and units for bone histomorphometry: a 2012 update of the report of the ASBMR Histomorphometry Nomenclature Committee. J. Bone Miner. Res. *28*, 2–17. https://doi.org/10.1002/jbmr.1805.

41. Li, B., and Dewey, C.N. (2011). RSEM: accurate transcript quantification from RNA-Seq data with or without a reference genome. BMC Bioinf. *12*, 323. https://doi.org/10.1186/1471-2105-12-323.

42. Dobin, A., Davis, C.A., Schlesinger, F., Drenkow, J., Zaleski, C., Jha, S., Batut, P., Chaisson, M., and Gingeras, T.R. (2013). STAR: ultrafast universal RNA-seq aligner. Bioinformatics *29*, 15–21. https://doi.org/10.1093/bioinformatics/bts635.

43. Love, M.I., Huber, W., and Anders, S. (2014). Moderated estimation of fold change and dispersion for RNA-seq data with DESeq2. Genome Biol. *15*, 550. https://doi.org/10.1186/s13059-014-0550-8.

44. Subramanian, A., Tamayo, P., Mootha, V.K., Mukherjee, S., Ebert, B.L., Gillette, M.A., Paulovich, A., Pomeroy, S.L., Golub, T.R., Lander, E.S., and Mesirov, J.P. (2005). Gene set enrichment analysis: a knowledge-based approach for interpreting genome-wide expression profiles. Proc. Natl. Acad. Sci. USA *102*, 15545–15550. https://doi.org/10.1073/pnas.0506580102.

45. Liberzon, A., Birger, C., Thorvaldsdóttir, H., Ghandi, M., Mesirov, J.P., and Tamayo, P. (2015). The Molecular Signatures Database (MSigDB) hallmark gene set collection. Cell Syst. *1*, 417–425. https://doi.org/10.1016/j.cels.2015.12.004.

46. Lyons, J.S., Iyer, S.R., Lovering, R.M., Ward, C.W., and Stains, J.P. (2016). Novel multi-functional fluid flow device for studying cellular mechanotransduction. J. Biomech. *49*, 4173–4179. https://doi.org/10.1016/j.jbiomech.2016.11.051.

STAR★METHODS

KEY RESOURCES TABLE

REAGENT or RESOURCE	SOURCE	IDENTIFIER
Antibodies		
Rabbit anti-mouse TLR4	Abcam	Ab13867
Alexa Fluor™ 488, Goat anti-rabbit IgG	Thermo Fisher	A-11034
Biological samples		
Fetal bovine serum	Corning	35-010-CV
Chemicals, peptides, and recombinant proteins		
Calcein, 10mg/kg	Sigma	C0875
Alizarin Red S, 30mg/kg	Sigma	A3882
Eukitt mounting medium	Sigma	03989
RNAlater	ThermoFisher	AM7020
TRIzol	ThermoFisher	15596026
BAY-11-7082	Sigma	B5556
Pyrrolidine dithiocarbamate	Sigma	P8765
TAK-242	Cayman Chemicals	13871
O.C.T compound	Tissue-Tek	4583
Vectashield Antifade mounting medium with DAPI	Vector labs	H-1200-10
a-Minimal Essential Medium for cell culture	Corning	15-012-CV
Penicillin/streptomycin antibiotic	Sigma	P4333
Critical commercial assays		
Qiagen RNeasy kit	Qiagen	74004
iScript cDNA synthesis kit	BioRad	1708890
Deposited data		
Raw bulk sequencing data	This paper	NCBI GEO GSE210597
Experimental models: Cell lines		
MC3T3-E1 Subclone 4	ATCC	CRL-2593
Primary calvarial osteoblasts	This paper	N/A
Experimental models: Organisms/strains		
$Tlr4^{fl/fl}$ mice	Jackson labs	024872
Osteocalcin-Cre+ mice	Jackson labs	019509
$Tlr4^{fl/fl}$; OC-Cre+ mice on a C57BL/6J background	This paper	N/A
NGF-EGFP mice	Kawaja et al.[37]	N/A
Oligonucleotides		
Primers for qPCR, see Table 1	IDT Technologies	N/A
Software and algorithms		
Prism 9	Graphpad	N/A
ImageJ	https://imagej.nih.gov/ij/index.html	N/A
GNU Octave	Octave.org	N/A
NRecon	Bruker	N/A
CTan	Bruker	N/A
Other		
Type I collagenase	Worthington Biochemical Corp.	4197

RESOURCE AVAILABILITY

Lead contact

Further information and requests for reagents and resources should be directed to and will be fulfilled by the lead contact, Ryan Tomlinson (ryan.tomlinson@jefferson.edu).

Materials availability

All materials in this study will be made available on request to the lead contact.

Data and code availability

- RNA sequencing data for this study is deposited in a publicly available database and the accession code for this data is GSE210597.
- This paper does not report original code.
- All data reported in this paper and any additional information required to reanalyze the data is available from the lead contact upon request.

EXPERIMENTAL MODEL AND SUBJECT DETAILS

Mouse strains

$Tlr4^{fl/fl}$; Osteocalcin (OC)-Cre+ mice (CKO) on a C57BL/6J background were generated for this study in accordance with IACUC of Thomas Jefferson University. These mice were generated by crossing mice carrying Tlr4 homozygous floxed alleles (Jackson Labs #024872) with mice carrying Cre recombinase driven by the osteocalcin promoter (Jackson Labs #019509). $Tlr4^{fl/fl}$ (WT) littermates were included as controls in the study. NGF-EGFP mice express EGFP under the control of the full-length mouse *Ngf* promoter.[37] All mice were housed at 72°F and fed a daily diet of rodent chow (LabDiet 5001). Unless otherwise noted, both male and female adult mice (16-20 weeks) were used for all experiments.

Cell lines and culture

The MC3T3-E1 Subclone 4 pre-osteoblast cell line was derived from ATCC (#CRL-2593). Primary osteoblasts were isolated from D0-D3 CKO and WT mice using standard techniques.[38] Briefly, neonatal calvaria were dissected, cut into pieces, washed in sterile PBS, and sequentially digested using 1.8 mg/mL type I collagenase (Worthington Biochemical Corp. #4197) to release the osteoblasts into solution. For loading experiments, cells were seeded in standard 96-well plates and cultured in complete media comprising α-Minimal Essential Medium (Corning #15-012-CV), 10% fetal bovine serum (Corning #35-010-CV) and 1% penicillin/streptomycin antibiotic (Sigma #P4333).

METHOD DETAILS

Skeletal preparations

P0 mice were euthanized by cervical dislocation and placed in ice-cold PBS. Immediately following euthanasia, pups were skinned and eviscerated. Following dehydration in ethanol and tissue permeabilization in acetone, skeletons were incubated for 3-4 days in a staining solution consisting of 0.3% Alcian blue stock and 0.1% alizarin red S stock at 37°C. Excess stain was removed by soft tissue hydrolysis in 1% potassium hydroxide, which enabled transparency and visualization of skeletal elements. Skeletons were imaged using a dissecting microscope.

In vivo mechanical loading

Axial forelimb compression of the right forelimb was performed using a material testing system (TA Instrument Electroforce 3200 Series III) with custom designed fixtures. Prior to loading, mice were anesthetized with 3% isoflurane and buprenorphine (0.12 mg/kg, IP), and they were maintained under 1.5% isoflurane for the duration of the loading protocol. Each mouse was loaded using a 2Hz sinusoidal, rest-inserted waveform with a peak force of 3N for 100 cycles each day over three consecutive days (D0-D2). This loading protocol has previously been shown to induce robust lamellar bone formation at the mid-shaft of the ulna.[39] The non-loaded left forelimb served as a contralateral control.

Histomorphometry

To assess load-induced bone formation by dynamic histomorphometry, adult (16-20 weeks) male and female mice were given calcein (10 mg/kg, Sigma C0875) on D3 and alizarin red s (30 mg/kg, Sigma A3882) on D8 of the loading protocol by IP injection. Animals were euthanized on D10. Forelimbs were dissected, fixed in 10% formalin overnight at 4°C, dehydrated in 70% ethanol, and embedded in polymethylmethacrylate. 100 micron thick sections from the mid-diaphysis of the ulnae were cut using a precision saw (Isomet 1000) and mounted on glass slides with Eukitt mounting medium (Sigma 03,989) and visualized by confocal microscopy (Zeiss). Bone formation parameters, including endosteal (Es) and periosteal (Ps) mineralizing surface (MS/BS), mineral apposition rate (MAR), and bone formation rate (BFR/BS), were quantified using ImageJ according to the guidelines of the ASBMR Committee for Histomorphometry Nomenclature.[40]

To characterize bone cells by static histomorphometry, 8-9 week old femurs were fixed, decalcified in 14% EDTA for 2 weeks at 4°C, and embedded in paraffin. 4 micron thick sections were stained with either standard H&E or tartrate-resistant acid phosphatase (TRAP) stain. Sections were imaged using a bright field microscope (EVOS M5000 imaging system). Three 20X regions of the femoral metaphysis were analyzed to determine average number of osteoblasts or osteoclasts per bone surface and osteocytes per bone area.

For immunofluorescent staining of TLR4 protein, adult mice were given three bouts of compressive loading, and forelimbs were harvested on D7 post loading on D0. Forelimbs were fixed, decalcified and embedded in paraffin, and 4 micron thick sections were cut from the mid-section of the ulnar diaphysis. Sections were deparaffinized, rehydrated, and treated with 0.05% citrate buffer for 30 min. Next, non-specific antigens were blocked with normal goat serum, before overnight incubation with a rabbit, anti-mouse TLR4 antibody (Abcam ab13867) at 4 °C. The next day, sections were washed and treated with a goat anti-rabbit IgG fluorescent secondary antibody (Alexa Fluor™ 488, Life Technologies) for 1 h. Sections were treated with a nuclear counterstain (Vectashield mounting medium, Vector Labs, Newark, CA) and imaged with a confocal microscope (Zeiss). Three high-powered 10X regions of the periosteum were analyzed to determine average number of TLR4 positive cells as a percentage of total periosteal cells.

To visualize NGF-EGFP expression, forelimbs from NGF-EGFP adult mice were harvested 3 h following one bout of compressive loading, fixed, decalcified, and embedded in O.C.T compound (Tissue-Tek), and 10 micron thick sections were cut from the mid-section of the ulnar diaphysis. Sections were mounted with media containing DAPI (Vectashield H1500) and imaged with a confocal microscope (Zeiss). The entire medial periosteal region was analyzed in ImageJ to determine area percentage of GFP in each section.

Micro computed tomography and three-point bending

For analysis of skeletal phenotype by microCT, the right femurs were dissected from adult mice and frozen at −20°C in PBS-soaked gauze. Each bone was scanned using a Bruker microCT analyzer fixed with a 1 mm aluminum filter, and with scanning parameters of 55 kV and 181 μA at a resolution of 12 microns. Bone scans were reconstructed using nRecon (Bruker), and aligned and analyzed using CTan (Bruker) for cortical and trabecular bone parameters. For mechanical testing of adult femurs with three-point bending, femurs were placed on custom fixtures with the condyles facing down and a span length of 7.6 mm measured with calipers. Femurs were then subjected to a monotonic displacement ramp of 0.1 mm/s until failure. Force and displacement data from the test as well as geometric parameters from microCT were analyzed using a custom GNU Octave script to derive structural and material properties.

RNA isolation and sequencing

The middle third of loaded and non-loaded ulnae from adult, male mice were harvested 3 h after a single bout of loading on D0 to extract RNA for whole transcriptome analysis. Bones were centrifuged to remove bone marrow, then stored in RNAlater (ThermoFisher) at −80 °C. Bone tissue was pulverized in TRIzol (ThermoFisher) to obtain uniform tissue homogenates, and total RNA was isolated from bone homogenates using the TRIzol method as per manufacturer's instructions. RNA was further purified using a Qiagen RNeasy kit (Qiagen) and samples with RIN values ranging from 5-8 were selected for sequencing. Illumina Stranded Total RNA libraries were prepared including Ribo-Zero Plus rRNA depletion as per the manufacturer's protocols. Libraries were sequenced on the Illumina NovaSeq 6000 using 2 × 100 base paired-end chemistry v1.5 reagents. The resulting reads in FASTQ format were aligned to the mouse genome version

GRCm38 with Gencode M19 transcript annotations using the RSEM-STAR pipeline.[41,42] Gene expression count files produced by RSEM were analyzed for differential expression using the DESeq2 package in R/Bioconductor software.[43] The Gene Set Enrichment Analysis (GSEA) pre-ranked tool was applied to genes ranked by their resulting DESeq2 test statistic to identify differentially regulated Hallmark gene-sets.[44,45] Additional visualization was performed using the R/Bioconductor EnhancedVolcano package (version 1.8.0).

In vitro fluid shear stress

To assess *Ngf* expression, MC3T3-E1 cell cultures were subjected to fluid shear stress of 1 mL/min for 0 (control), 10, 15, 30, and 60 min using a previously developed microfluidics fluid flow device[46] coupled to a standard peristaltic pump with 1.6 mm (ID) polyethylene tubing. To determine the requirement of the NF-κB signaling pathway following loading, osteoblast cultures were supplemented with either 5 μM BAY 11-7082 (Sigma) or 50 μM pyrrolidine dithiocarbamate (PDTC, Sigma) 1 h before loading for 60 min at 1 mL/min. To determine the role of TLR4 signaling, cultures were supplemented with either 5 or 10 μM TAK-242 (Cayman Chemicals) 2 h before loading for 60 min at 1 mL/min. Cells were harvested 1 h following loading in all inhibitor experiments. Control groups were not loaded and/or treated with DMSO (vehicle).

Gene expression analysis

Total RNA from cell cultures was isolated using the TRIzol method, purified with the Qiagen RNeasy kit, and quantified using a NanoDrop spectrophotometer. RNA was reverse transcribed using iScript cDNA synthesis kit (BioRad), and amplified using SYBR Green biochemistry with the QuantStudio 3 real-time PCR system (Applied Biosystems). Relative gene expression was quantified using the ΔΔCT method, using GAPDH as a reference gene. Primer sequences were designed using Primer-BLAST and purchased from IDT Technologies. A complete list of primer sequences is provided in table.

Oligonucleotide primers used for qRT-PCR

Target	Forward (5′-3′)	Reverse (5′-3′)
Tlr4 exon 3	CTCTAGCCCACTGCTTCAGG	TCATCTGCCTGAACCCATTAC
Tlr4	AATCCCTGCATAGAGGTAGTTCC	CTTCAAGGGGTTGAAGCTCAG
Wnt1	GTAGCTGAAGAGTTTCCGAGTT	GGCAGAGACAAGGAGAATGTAG
Wnt7b	GGAGAAGCAAGGCTACTACAAC	CATCCACAAAGCGACGAGAA
Ngf	CAGTGAGGTGCATAGCGTAAT	CTCCTTCTGGGACATTGCTATC
Nfkb1	ATGGCAGACGATGATCCCTAC	TGTTGACAGTGGTATTTCTGGTG
RelB	GCCGAATCAACAAGGAGAGCG	CATCAGCTTGAGAGAAGTCGGCA
Gapdh	AGGTCGGTGTGAACGGATTTG	TGTAGACCATGTAGTTGAGGTCA

QUANTIFICATION AND STATISTICAL ANALYSIS

Data was collected in a blinded fashion from all animals in the study, unless removed prior to analysis due to illness or injury after consultation with veterinarian staff. After data collection, outlier analysis was performed using Grubbs' test if necessary. For *in vivo* comparisons of bone formation parameters in loaded versus non-loaded bone, two-way ANOVA was used with post hoc Tukey's tests. For analysis of skeletal phenotype, two-tailed, unpaired t-tests were used. Multiple group means for *in vitro* experiments were compared using one-way ANOVA with post hoc Tukey's tests (adjusted $p \leq 0.05$). Statistical analysis was carried out in Prism 9 (Graphpad).